Soft Matter

PAPER

View Article Online
View Journal

Cite this: DOI: 10.1039/c5sm01597a

A geometric model for the periodic undulation of a confined adhesive crack

Zhiyan Wei[a] and L. Mahadevan*[abc]

Received 28th June 2015,
Accepted 25th November 2015

DOI: 10.1039/c5sm01597a

www.rsc.org/softmatter

Inspired by experiments on the instability of confined interfacial cracks, we construct a minimal mathematical model based on symmetry arguments that can reproduce the form of the crack front in a confined domain. We show that the model can be interpreted in terms of the buckling and post-buckling response of a compressed elastica with a nonuniform bending stiffness that is adhered to a linearly elastic substrate. The model has three parameters that allow us to capture the primary wavelength associated with the onset of an undulatory instability of a straight crack front, as well as the finger amplitudes and finger widths in the nonlinear development of the instability. We determine these parameters using an optimization procedure that minimizes the square error between the computed profile and experimental observations. The results of this procedure yield numerical solutions that agree well with the finger profiles experimentally observed in films of different thicknesses. Our approach shows the efficacy of simple models based on symmetry in explaining interfacial instabilities governed by different physical mechanisms.

1 Introduction

Interfacial instabilities lead to a host of patterns in nature. Examples include the growth of crystals *via* the process of solidification,[1] the hydrodynamic free-surface instability between liquids of different viscosities in a narrow gap,[2,3] the analogous elastic instability at the meniscus in a stressed thin film,[4,5] crack growth in solid materials,[6–8] and various biological analogues.[9] The evolution of the moving interface is usually determined in terms of the solution of a free boundary problem that couples the geometry of the interface to the bulk field equations associated with different physical and chemical phenomena that drive it. One approach to these problems, which has been particularly successful, is using phase field models[1,10,11] in solidification dynamics,[12] fracture dynamics,[13,14] viscous fingering[15] and vesicle dynamics.[16] A closely related approach is the use of geometrical models[9,17–22] that are motivated by symmetry arguments to write down phenomenological laws for the motion of the interface. This class of models is not meant to fully reproduce the realistic intricacies of the long-time development of the system, but as they are based on general symmetry and geometic considerations, they can capture a wide variety of growth dynamics, even though the physical origins of competing stabilizing and destabilizing forces acting on the moving boundary depend on the particular system under investigation.[18,21,22] These models can sometimes be derived using weakly nonlinear analysis[23] and by using the methods of multiple scale asymptotics, but are often used successfully beyond their nominal regime of validity.

In elasticity, a crack is represented as an interface, and there has been much work on the stability of crack in a bulk solid[11,19,24] under static and dynamic conditions, usually in the presence of periodic or random material heterogeneity or anisotropy. This work takes the form of linear stability analysis[25,26] combined with phase field-like approaches[27,28] to follow the nonlinear evolution of crack fronts, while attempts to write down geometrical models for the nonlinear growth and saturation in these contexts[19] have not met with much success. Here, we revisit this question in the case of an interfacial crack in a confined elastic film which becomes unstable to undulatory fingers;[29,30] the effect of geometric confinement localizes the response of the solid to out-of-plane displacements, and this leads to undulations in the crack front.

In Fig. 1(a), we show the schematic for such an experiment where a flexible cover-slip is peeled from a soft, thin elastic adhesive film that is attached firmly to a rigid substrate. Fig. 1(b) shows that the adhesive failure between the cover-slip and the thin film manifests itself in the form of periodic finger-like undulations, which develop during the opening of the crack and remain stable even after the crack comes to a complete rest.[29] Previous work[30] has shown that the onset of the wavy crack front depends on the ratio of two length scales:

[a] Paulson School of Engineering and Applied Sciences, Harvard University, Cambridge, MA 02138, USA. E-mail: lm@seas.harvard.edu
[b] Department of Physics, Harvard University, Cambridge, MA 02138, USA
[c] Kavli Institute for Nano-Bio Science and Technology, Wyss Institute for Bio-inspired Engineering, Harvard University, Cambridge, Massachusetts 02138, USA

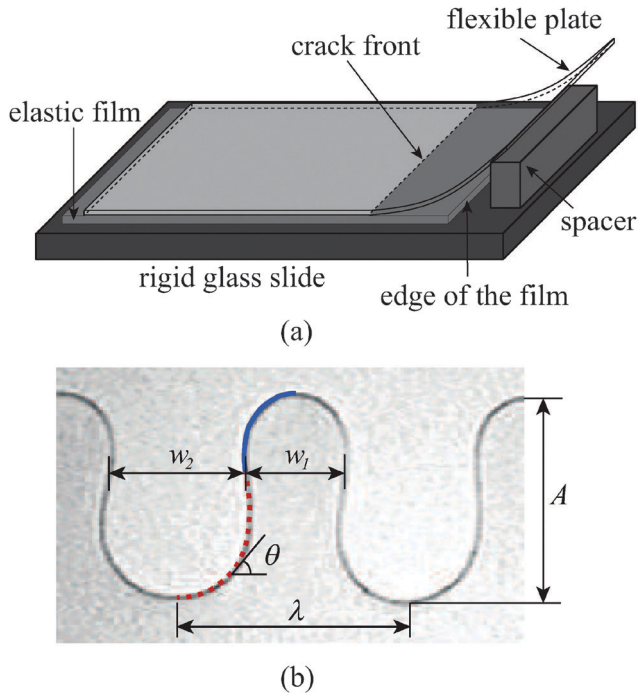

Fig. 1 (a) Schematic of the experimental setup used in ref. 29. (b) the crack front[29] loses stability to an undulatory mode when the confinement parameter $\alpha = (B/\mu h^3)^{1/3}$ is large enough.[30] Here B is the bending stiffness of the flexible plate, μ is the shear modulus of the elastic film, h is the thickness of the film, A is the amplitude of the finger, λ is the wavelength of the undulatory crack front, and w_1 and w_2 are the widths of the fingers protruding down and up respectively, θ (>0 is counter-clockwise) is the angle made by the tangent of the plane curve with respect to the horizontal direction, and increases from 0 to its maximum value along the red dashed line and decreases from its maximum value to 0 along the blue solid curve. Experimental image adapted from ref. 29.

the film thickness h and an elastic length $(B/\mu)^{1/3}$ defined by the bending stiffness B of the cover-plate and the shear modulus μ of the film. A more detailed analysis predicts that the wavelength of the undulation λ scales linearly with h, with $\lambda \approx 3.4h$, which is in reasonable agreement with the corresponding experimental values of $\lambda_{\mathrm{exp}} \approx 4h$.[29] However, the linear theory loses its predictive power when the crack front evolves into a set of finite amplitude fingers, a regime in which only a scaling analysis has so far been used to estimate the characteristic size of the fingers.[31] Here, we show that it is possible to explain the nonlinear evolution of the crack in terms of a geometric scalar model that captures the quantitative features of the interfacial crack front in a minimal mathematical setting.

2 Geometric model

The interfacial crack front is a plane curve which we parameterize in terms of (s, θ), where s is the arclength of the curve and θ is the angle made by the tangent vector of the curve with respect to the horizontal direction. Inspired by the scale separation in the thin elastic film, since the film thickness is much smaller than the film width, we write down a phenomenological growth law for the crack front in terms of the evolution of a $2D$ curve with time given by

$$\theta_t = c_1\left(\theta - \frac{\theta^3}{\theta_{\mathrm{m}}{}^3}\right) + [c_2 + f(\theta_s)]\theta_{ss} + c_3\int_0^s \mathrm{d}s_2\int_0^{s_2}\theta(s_1)\mathrm{d}s_1, \quad (1)$$

where $A_b = \partial A/\partial b$, $s \in [0,L]$, and the total arc length $L(t)$ is a function to be determined, θ_{m} is the saturated magnitude of θ after the fingers reaches a steady state. The coefficients c_1, c_2 and c_3 are positive, and we will explain their mathematical significance, as well as that of function $f(\theta_s)$, in the following discussion. The assumption of gradient flow associated with overdamped dynamics in eqn (1) is motivated by simplicity. As our primary goal is to focus on the equilibrium shapes of the crack front, we will in fact focus only on the quasi-static evolution of the crack. To motivate the right-hand side, we note that we have kept terms to $O(\theta^3)$, and further that the equation is symmetric under the transformation $\theta \to -\theta$ and $s \to -s$ (when $f(\theta_s)$ vanishes), approximately consistent with the experimental observations when the finger amplitudes are very small. As we will see, the term $f(\theta_s)$ breaks symmetry in a way that allows us to explain the observations quantitatively when figure amplitudes become large.

To understand the linear terms of the right-hand side of eqn (1) we use an analogy to the archetypal instability in elasticity of a compressed elastic strut, the elastica[32] with a uniform bending stiffness but the one that is adhered to a linearly elastic substrate. Its equilibrium shape $y(s)$ is given by the equation

$$By_{ssss} + Py_{ss} + Ey = 0, \quad (2)$$

where the elastica is initially aligned in the horizontal direction, B is its bending stiffness, P is the compressive force acting in the horizontal direction, and E is the elastic modulus of the substrate. Since $y_s = \theta$ in a linearized setting, where θ is the angle made by the tangent vector of the elastica with the horizontal direction, eqn (2) can be rewritten in terms of θ as $B\theta_{sss} + P\theta_s + E\int_0^s\theta(s_1)\mathrm{d}s_1 = 0$, which can be integrated once with respect to s to get

$$B\theta_{ss} + P\theta + E\int_0^s \mathrm{d}s_2\int_0^{s_2}\theta(s_1)\mathrm{d}s_1 = 0. \quad (3)$$

Comparing eqn (3) with eqn (1), we see that the coefficients $c_1 \equiv P$, $c_2 \equiv B$ and $c_3 \equiv E$, *i.e.* c_1 corresponds to the buckling force on the crack front that transitions from a straight "elastica" to an undulatory one, and the competition between the bending resistance of the elastica and the elastic resistance of the substrate selects the optimal wavelength of the undulation, $2\pi(c_2/c_3)^{1/4}$. Of course, the crack front is not physically analogous to an elastic filament. Nevertheless, we see that transverse displacements in the thin incompressible elastic film lead to effective in-plane compressive strains that cause the crack front to undulate when the stress-intensity factor switches sign,[30] so that our geometrical model does indeed capture the essence of this instability.

When the undulation evolves into a finite amplitude, the fingers are still symmetric although they may have different

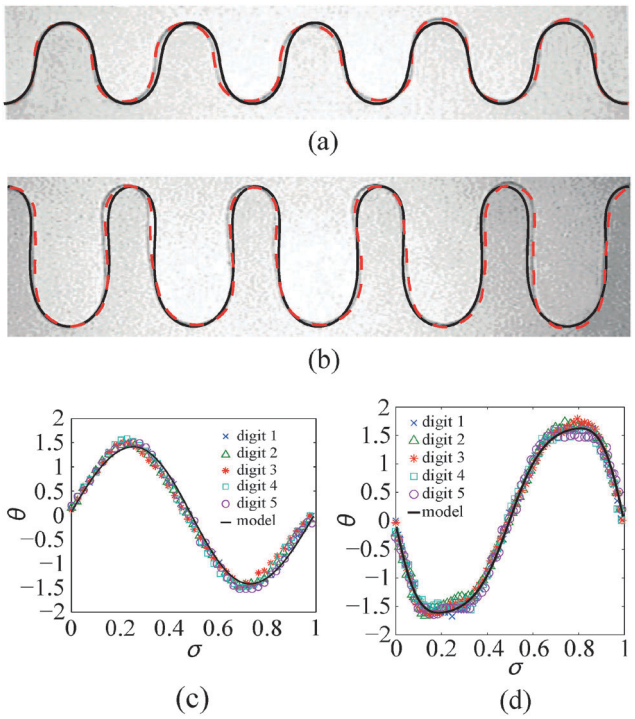

Fig. 2 Experimental images from ref. 29 show the saturated interfacial cracks that form finite amplitude fingers for two different values of film thickness. The red dashed curve traces the interfacial crack, and the black solid curve is obtained by solving the geometric model, eqn (4)–(6). Parameters are chosen by the CMA-ES method to generate 5 fingers that minimize the square error between the computed profile and the experimental result. (a) $\theta_m = 1.022\pi$, $\varepsilon = 0.022$, $\varepsilon_1 = 6.222 \times 10^{-3}$. (b) $\theta_m = 0.5122\pi$, $\varepsilon = 0.016$, $\varepsilon_1 = 0.0101$. In both cases, the +sign is adopted in eqn (5) when $\theta_\sigma > 0$. (c) and (d) Comparisons of the tangent angle $\theta(\sigma)$ of a single digit obtained from experiment and our geometrical model, as a function of $\sigma \in [0,1]$ the scaled arclength coordinate. (c) Corresponds to the example of (a) and (d) corresponds to the example of (b).

widths (Fig. 1(b)). This means that the peak and the valley of $\theta(s)$ are equal in magnitude but opposite in sign, and the reflection symmetry s to $-s$ in $\theta(s)$ may be broken (*i.e.* the arc length of the red dotted curve, along which $\theta(s)$ increases from 0 to its maximum value, and that of the blue solid curve, along which $\theta(s)$ decreases from its maximum value to 0, are not necessarily the same, as shown in Fig. 1(b)). A minimal approach to the saturation of the amplitude demands the choice $\theta^3/\theta_m{}^3$ in eqn (1) in light of the symmetry $\theta \to -\theta$. The same symmetry also exists in the post-buckling shape of the elastica, characterized by the nonlinear version of eqn (3) $D\theta_{ss} + P\sin(\theta) + E\int_0^s ds_2 \int_0^{s_2} \sin\theta(s_1) ds_1 = 0$, where we see that θ^3 is also the first nonlinear term in the expansion of $\sin\theta$. The peak and valley of $\theta(s)$ scale with parameter θ_m; by tuning this term we can control the finger profile to either be a graph or not. Finally, we note that to break the reflection symmetry in $\theta(s)$, we introduce the coefficient $f(\theta_s)$ in eqn (1) thereby allowing the patterns to form fingers of different widths. From the perspective of the elastica, the coefficient $c_2 + f(\theta_s)$ effectively corresponds to the nonuniform bending stiffness of an elastica that depends on θ_s. Thus, when an elastica is subjected to the same compressive force, it is bent into a smaller curvature at places where it is stiffer, *i.e.* $f(\theta_s) > 0$, resulting in a finger with a larger width.

Using the rescaled variables $\tau = c_1 t$ and $\sigma = s/L \in [0,1]$, eqn (1) can be written in the dimensionless form as

$$\theta_\tau = \left(\theta - \frac{\theta^3}{\theta_m{}^3}\right) + \left[\varepsilon^2 + f(\theta_\sigma)\right]\theta_{\sigma\sigma} + (2\pi n)^4 \varepsilon^2 \int_0^\sigma d\sigma_2 \int_0^{\sigma_2} \theta(\sigma_1) d\sigma_1, \tag{4}$$

where $\varepsilon = \sqrt{c_2/c_1}$ with c_1 and c_2 being the coefficients in eqn (1), and n is the number of fingers in the domain. Although the time scale c_1 is a free parameter that potentially provides the freedom to capture the dynamical evolution, we only compare our model with the experiments where stationary crack interfaces were studied. We use time evolution only as a numerical tool to solve the equation to reach equilibrium. The simplest form of $f(\theta_\sigma)$ is

$$f(\theta_\sigma) = \begin{cases} \pm\varepsilon_1{}^2 & \text{if } \theta_\sigma > 0 \\ \mp\varepsilon_1{}^2 & \text{if } \theta_\sigma < 0 \\ 0 & \text{otherwise} \end{cases}, \tag{5}$$

which allows us to independently control the widths of fingers $\sim(\varepsilon^2 \pm \varepsilon_1{}^2)^{1/2}$. The $\pm$sign allows us to account for the experimental fact that the finger protruding upward is fatter (or thinner). As eqn (4) is autonomous in σ, it is translationally invariant for periodic boundary conditions. To determine the increasing contour length L, we use the experimental fact that the spacing of the fingers does not change as they grow, which is enforced by the constraint

$$L\int_0^1 \cos\theta \, d\sigma = L_0, \tag{6}$$

where L_0 is the initial length of the straight crack front, and is scaled by the thickness of the thin film h. For example, in Fig. 2(a), there are 5 fingers, so we set $n = 5$ in eqn (4) and $L_0 = 20$ in eqn (6) as $\lambda = 4$.

3 Results

With the periodic boundary conditions and random perturbations on $\theta = 0$ as the initial condition, we show that the steady-state solution of eqn (4)–(6) reproduces the profile of the crack front. The 3 fitting parameters in this model, ε, ε_1 and θ_m, are determined using an optimization framework. We start with an initial guess of the parameters, and use the covariance matrix adaptation evolutionary strategy (CMA-ES) method[33,34] to converge to an optimal set of solutions that minimize the square error between the computed profile and the experimental results. The CMA-ES is a stochastic derivative-free optimization method for non-linear or non-convex continuous optimization problems. By incrementally increasing the probability of previously successful candidate solutions, we iteratively perform the following three steps: (1) sample p new n-dimensional solutions following the distribution with the updated mean

and covariance (with step size built in), (2) evaluate the cost function and re-order the sampled solutions based on their fitness, and (3) update the internal state variables, including the mean, the isotropic and anisotropic evolution path, the covariance matrix, and the step size, based on the q best out of p solutions, until we have converged to the best fit of the data.

Fig. 2(a) and (b) show experimental pictures of the crack front taken from ref. 29 corresponding to different film thicknesses. In (a) the finger profile takes the form of a graph while in (b) it is not a graph and must be parametrized in terms of arc-length. In both cases, the red curve traces the front, and the black solid curve represents the numerical solutions solved from eqn (4)–(6). As the solution is periodic, we consider a single finger from the numerical result, and compare the computed θ with the 5 fingers from the experiment, as shown in Fig. 2(c) and (d), which correspond to the examples of (a) and (b) respectively. We see that the amplitude, the width, the spacing and the tangent angle of the fingers are all captured well. Our approach thus allows us to use just 3 fitting parameters to quantitatively reproduce a class of crack fronts with different shapes.

4 Conclusions

Complex interfacial patterns often arise from simple causes. However, even these simple causes lead to mathematical models that are formidable, involving free boundary problems. Using concepts from symmetry and optimization, we have shown that it is possible to compress the information associated with a particular interfacial instability that arises from peeling a flexible elastic plate off a soft, thin confined adhesive film, where the adhesive failure occurs *via* the loss of adhesion at one of the surfaces attached to the adhesive, and an undulating crack front may appear and evolve into a 2D rippling pattern. Our minimal mathematical model, eqn (4) and (5) has 3 fitting parameters ε, ε_1 and θ_m that allow us to capture the wavelength at the onset of undulation, the finger amplitudes and widths of the crack front.

Our model can be interpreted physically in terms of the buckling and post-buckling response of an initially straight elastica that has a nonuniform bending stiffness and is adhered to a linearly elastic substrate. Our model is also similar to the classic Allen–Cahn equation,[35,36] with two important differences: the nonlocal double integral that corresponds to the effective elastic resistance of the substrate that prevents the pattern from coarsening indefinitely, and $f(\theta_\sigma)$ that is responsible for breaking the reflection symmetry of $\theta(s)$ and results in fingers of different widths. More generally, our model describes a class of phase separation phenomena with an eventual arrest at a characteristic size that include pattern formation of a two-phase epitaxial monolayer grown on an elastic substrate,[37] the evolution of nanoporosity in dealloying,[38] and the continuous model used to describe the capillarity-driven and elastically limited coarsening of a one-dimensional array of lamellae.[39] These models are similar mathematically because they share the same embedded symmetries, even though they are based on different physical mechanisms. More detailed studies can be carried out to generalize the symmetry arguments to describe a wide range of periodically moving interfaces by designing the effective bending stiffness of the elastica $c_2 + f$, or alternatively designing the effective substrate modulus c_3 in eqn (4) to be a spatial-temporal field.

We thank Mattia Gazzola for many discussions on the CMA-ES method. We thank the Harvard-MRSEC DMR-1420570, and the MacArthur Foundation (LM) for support.

References

1 J. S. Langer, *Rev. Mod. Phys.*, 1980, **52**, 1–28.
2 P. Saffman and G. Taylor, *Proc. R. Soc. London, Ser. A*, 1958, **245**, 312–329.
3 G. Homsy, *Annu. Rev. Fluid Mech.*, 1987, **19**, 271–311.
4 B. Saintyves, O. Dauchot and E. Bouchaud, *Phys. Rev. Lett.*, 2013, **111**, 047801.
5 J. Biggins, B. Saintyves, Z. Wei, E. Bouchard and L. Mahadevan, *Proc. Natl. Acad. Sci. U. S. A.*, 2013, **110**, 12545–12548.
6 J.-Y. Faou, G. Parry, S. Grachev and E. Barthel, *Phys. Rev. Lett.*, 2012, **108**, 116102.
7 A. Yuse and M. Sano, *Nature*, 1993, **362**, 329–331.
8 M. Lamblet, E. Verneuil, T. Vilmin, A. Buguin, P. Silberzan and L. Léger, *Langmuir*, 2007, **23**, 6966–6974.
9 A. T. Winfree, *The Geometry of Biological Time*, Springer, 2nd edn, 2001.
10 N. Provatas, N. Goldenfeld and J. Dantzig, *J. Comput. Phys.*, 1999, **148**, 265–290.
11 A. Karma and W.-J. Rappel, *Phys. Rev. E: Stat. Phys., Plasmas, Fluids, Relat. Interdiscip. Top.*, 1998, **57**, 4323.
12 W. J. Boettinger, J. A. Warren, C. Beckermann and A. Karma, *Annu. Rev. Mater. Res.*, 2002, **32**, 163–194.
13 A. Karma, D. A. Kessler and H. Levine, *Phys. Rev. Lett.*, 2001, **87**, 045501.
14 V. Hakim and A. Karma, *J. Mech. Phys. Solids*, 2009, **57**, 342–368.
15 R. Folch, J. Casademunt, A. Hernández-Machado and L. Ramírez-Piscina, *Phys. Rev. E: Stat. Phys., Plasmas, Fluids, Relat. Interdiscip. Top.*, 1999, **60**, 1734–1740.
16 T. Biben, K. Kassner and C. Misbah, *Phys. Rev. E: Stat., Nonlinear, Soft Matter Phys.*, 2005, **72**, 041921.
17 R. C. Brower, D. A. Kessler, J. Koplik and H. Levine, *Phys. Rev. E: Stat. Phys., Plasmas, Fluids, Relat. Interdiscip. Top.*, 1984, **29**, 1335–1342.
18 D. A. Kessler, J. Koplik and H. Levine, *Adv. Phys.*, 1988, **37**, 255–339.
19 J. A. Hodgdon and J. P. Sethna, *Phys. Rev. B: Condens. Matter Mater. Phys.*, 1993, **47**, 4831–4840.
20 P. Grindrod, M. A. Lewis and J. D. Murray, *Proc. R. Soc. London, Ser. A*, 1991, **433**, 151–164.
21 R. E. Goldstein, D. J. Muraki and D. M. Petrich, *Phys. Rev. E: Stat. Phys., Plasmas, Fluids, Relat. Interdiscip. Top.*, 1996, **53**, 3933–3957.

22 M. Anderson, D. Srolovitz, G. Grest and P. Sahni, *Acta Metall. Mater.*, 1984, **32**, 783–791.
23 R. B. Hoyle, G. B. McFadden and S. H. Davis, *Philos. Trans. R. Soc., A*, 1996, **354**, 2915–2949.
24 H. Gao and J. R. Rice, *J. Appl. Mech.*, 1989, **56**, 828–836.
25 J.-B. Leblond, A. Karma and V. Lazarus, *J. Mech. Phys. Solids*, 2011, **59**, 1872–1887.
26 V. Lazarus, *J. Mech. Phys. Solids*, 2011, **59**, 121–144.
27 F. Corson, M. Adda-Bedia, H. Henry and E. Katzav, *Int. J. Fract.*, 2009, **158**, 1–14.
28 A. J. Pons and A. Karma, *Nature*, 2010, **464**, 85–89.
29 A. Ghatak, M. K. Chaudhury, V. Shenoy and A. Sharma, *Phys. Rev. Lett.*, 2000, **85**, 4329–4332.
30 M. A. Bedia and L. Mahadevan, *Proc. R. Soc. London, Ser. A*, 2006, **462**, 3233–3251.
31 T. Vilmin, F. Ziebert and E. Raphael, *Langmuir*, 2010, **26**, 3257–3260.
32 A. E. H. Love, *A Treatise on the Mathematical Theory of Elasticity*, The University Press, 1906.
33 N. Hansen and A. Ostermeier, *Evol. Comput.*, 2001, **9**, 159–195.
34 N. Hansen, S. D. Muller and P. Koumoutsakos, *Evol. Comput.*, 2003, **11**, 1–18.
35 S. M. Allen and J. W. Cahn, *Acta Metall. Mater.*, 1972, **20**, 423.
36 S. M. Allen and J. W. Cahn, *Scr. Metall. Mater.*, 1973, **7**, 1261.
37 W. Lu and Z. Suo, *J. Mech. Phys. Solids*, 2001, **49**, 1937–1950.
38 J. Erlebacher, M. Aziz, A. Karma, N. Dimitrov and K. Sieradzki, *Nature*, 2001, **410**, 450–453.
39 Z. Wei and L. Mahadevan, *Europhys. Lett.*, 2014, **106**, 14002.